Band alignment of atomic layer deposited SiO_2 on (010) $(Al_{0.14}Ga_{0.86})_2O_3$

Chaker Fares, F. Ren, Eric Lambers, David C. Hays, B. P. Gila, and S. J. Pearton

Citation: Journal of Vacuum Science & Technology B **36**, 061207 (2018); doi: 10.1116/1.5052620
View online: https://doi.org/10.1116/1.5052620
View Table of Contents: http://avs.scitation.org/toc/jvb/36/6
Published by the American Vacuum Society

Band alignment of atomic layer deposited SiO_2 on (010) $(Al_{0.14}Ga_{0.86})_2O_3$

Chaker Fares,[1] F. Ren,[1] Eric Lambers,[2] David C. Hays,[2] B. P. Gila,[2] and S. J. Pearton[3,a)]
[1]*Department of Chemical Engineering, University of Florida, Gainesville, Florida 32611*
[2]*Nanoscale Research Facility, University of Florida, Gainesville, Florida 32611*
[3]*Department of Materials Science and Engineering, University of Florida, Gainesville, Florida 32611*

(Received 20 August 2018; accepted 16 October 2018; published 30 October 2018)

The $(Al_xGa_{1-x})_2O_3/Ga_2O_3$ system is attracting attention for heterostructure field effect transistors. An important device design parameter is the choice of gate dielectric on the $(Al_xGa_{1-x})_2O_3$ and its band alignment at the heterointerface. The valence band offset at the $SiO_2/(Al_{0.14}Ga_{0.86})_2O_3$ heterointerface was measured using x-ray photoelectron spectroscopy. The SiO_2 was deposited by atomic layer deposition (ALD) onto single-crystal β-$(Al_{0.14}Ga_{0.86})_2O_3$ grown by molecular beam epitaxy. The bandgap of the SiO_2 was determined by reflection electron energy loss spectroscopy as 8.7 eV, while high resolution XPS data of the O 1s peak and onset of elastic losses were used to establish the $(Al_{0.14}Ga_{0.86})_2O_3$ bandgap as 5.0 eV. The valence band offset was determined to be 1.60 ± 0.40 eV (straddling gap, type I alignment) for ALD SiO_2 on β-$(Al_{0.14}Ga_{0.86})_2O_3$. The conduction band offset was 2.1 ± 0.08 eV, providing for a strong electron transport restriction. *Published by the AVS.*
https://doi.org/10.1116/1.5052620

I. INTRODUCTION

β-Ga_2O_3 is a wide bandgap semiconductor (~4.9 eV) with properties suited to power electronics, truly solar-blind UV detection, and extreme environment applications.[1–14] The β monoclinic polymorph of Ga_2O_3 is the most prominent of the five phases of this material, and crystals up to 4 in. in diameter are commercially available. Ga_2O_3 has the potential to surpass GaN (bandgap 3.4 eV) for extreme environment operation. Kim *et al.*[15] have already shown operation of a nanobelt field effect transistor (FET) device from room temperature to 250 °C with no hysteresis of the device, and higher current and transconductance at elevated temperatures. Promising device performance has been reported for rectifiers, transistors, and solar-blind photodetectors on bulk, epitaxial and thin flakes of β-Ga_2O_3.[6–13,16–21] Ga_2O_3 has a theoretical field breakdown of 8 MV/cm, with experimental values reaching 3.8 MV/cm[3], surpassing the theoretical limit of GaN at 3.3 MV/cm. The current record of reverse breakdown of a vertical Schottky diode is 2300 V,[22] and the highest reported breakdown for a nonplanar device channel was set using a Ga_2O_3 FinFET at 612 V using Al_2O_3 as the gate dielectric.[16,18] The only disadvantage in Ga_2O_3's material properties is the relatively low thermal conductivity.[2,3]

Across all these applications, understanding and properly selecting a gate dielectric either in metal-oxide-semiconductor field effect transistor (MOSFET), metal-insulator-semiconductor field effect transistor, or diode design is required. With selection of a gate dielectric, generally at least a 1 eV difference between the insulating material on the gated area and the channel semiconductor is preferred for performance, as that difference will provide a sufficient energy barrier to hole and electron leakage current.[2,3,6] The majority of published MOSFET work on Ga_2O_3 has typically been either atomic layer deposited (ALD) Al_2O_3 or HfO_2 or ALD and plasma enhanced chemical vapor deposited SiO_2 and Al_2O_3 as the gate dielectrics, as they provide sufficient conduction band difference, reported from 1.5 to 3.1 eV.[23–36]

Additional bandgap tunability can be achieved through incorporation of Al into β-Ga_2O_3, leading to β-$(Al,Ga)_2O_3$ monoclinic phase alloys with the bandgap tuned from 4.8 to 6 eV.[16–24] This enables heterostructure designs such as modulation-doped electron channels, quantum wells, and superlattices.[16–21] A number of reports of modulation-doped field effect transistors using β-$(Al_xGa_{1-x})_2O_3/Ga_2O_3$ heterostructures show effective quantum confinement of electrons at the interface.[16–21] These devices require robust gate dielectrics. While band offsets for SiO_2 on $(Al_xGa_{1-x})_2O_3$ grown by pulsed laser deposition (PLD) have been reported for various values of x,[25] it is of interest to get results on molecular beam epitaxy (MBE)-grown layers, which should have better prospects of producing device-quality material.

There is typically variability reported in the literature for both valence and conduction band offsets on oxides such as indium gallium zinc oxide, Ga_2O_3, and $(Al_xGa_{1-x})_2O_3$ due to various effects,[37,38] which may include metal contamination in the deposited dielectric (especially in sputtered films), interface disorder, differences in dielectric composition as a result of different deposition methods or precursors, carbon/hydrogen contamination, annealing, stress/strain, and the type of surface termination. In some cases, these result in differences in the bandgap of the dielectric and thus affect the conduction band offset. Generally, the valence band offset is measured directly, and the conduction band offset is calculated from the difference between that and the bandgaps.[39,40] However, the valence band offset can also be affected by most of these same issues. The use of ALD deposited dielectrics minimizes most of these effects and provides a more controlled method for making the heterostructure samples for determining the band alignment.

In this paper, we report on the determination of the band alignment in the $SiO_2/(Al_{0.14}Ga_{0.86})_2O_3$ heterostructure, in which the SiO_2 was deposited by ALD. We employ XPS to

a)Electronic mail: spear@mse.ufl.edu

determine the valence band offsets and by measuring the respective bandgaps of the SiO_2 (8.7 eV) and β-$(Al_{0.14}Ga_{0.86})_2O_3$ (5.0 eV), we were able to determine the conduction band offset in the heterostructures and determine the band alignment.

II. EXPERIMENT

The SiO_2 was deposited by ALD on $(Al_{0.14}Ga_{0.86})_2O_3/Ga_2O_3$ structures and also quartz substrates. The latter were used for dielectric constant and composition measurements. Both thick (200 nm) and thin (1.5 nm) layers of the dielectrics were deposited to be able to measure both bandgaps and core levels on the β-$(Al_{0.14}Ga_{0.86})_2O_3$. For substrate cleaning predeposition, the following rinse sequence was employed: acetone, isopropyl alcohol, N_2 dry, and finally ozone exposure for 15 min. After substrate cleaning, samples were directly loaded into the ALD system within a clean room environment. Potential contamination of deposited films can influence the bandgap and offset of the dielectric material. To minimize this problem, the SiO_2 layers were deposited at 200 °C in a Cambridge Nano Fiji 200, a remote plasma atomic layer deposition tool, using an inductively coupled plasma source at 300 W. Atomic layer deposition is an effective method for band offset studies, because it can be utilized with a remote plasma to reduce contamination effects and also provides minimal disruption to the heterointerface due to reduced ion damage from using a remote source. The SiO_2 layers were deposited using precursors of tris (dimethylamino) silane and O_2 at a deposition rate of 0.63 A/cycle. After ALD deposition, the samples were transferred directly to the XPS system. These films were deposited onto epi $(Al_{0.14}Ga_{0.86})_2O_3$ that was grown by molecular beam epitaxy. These aluminum gallium oxide layers were doped with Si to produce an n-type carrier density of 10^{17} cm^{-3} and were 55 nm thick. This represents an advance in n-type doping capability because Si source material can suffer oxidation during growth unless precautions are taken in terms of shuttering the Si source and preheating prior to actual opening of the shutter to avoid this issue. The carrier concentration was determined by electrochemical capacitance-voltage profiling at a frequency of 740 Hz on calibration samples and the composition was determined by x-ray diffraction on these same samples. The latter composition was confirmed by ion microprobe data. These epitaxial layers were grown on top of Sn-doped $(6.3 \times 10^{18}$ $cm^{-3})$ bulk β-phase Ga_2O_3 single-crystal substrates (500 μm thick) with (010) surface orientation (Tamura Corporation, Japan) grown by the edge-defined film-fed growth method. The heterostructure sample is shown schematically in Fig. 1.

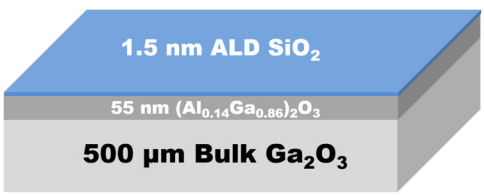

FIG. 1. Composition and corresponding thicknesses of materials used in this study.

To obtain the valence band offsets, XPS survey scans were performed to determine the chemical state of the SiO_2 and β-$(Al_{0.14}Ga_{0.86})_2O_3$ and identify peaks for high resolution analysis.[39,40] An ULVAC PHI XPS with an aluminum x-ray source (energy 1486.6 eV) with source power 300 W was used, with an analysis area of 20 μm in diameter, a take-off angle of 50°, and an acceptance angle of ±7°. The electron pass energy was 23.5 eV for the high resolution scans and 93.5 eV for the survey scans. The approximate escape depth (3λ sin θ) of the electrons was 80 Å. All of the peaks are well defined in this system.

Charge compensation was performed using an electron flood gun. The charge compensation flood gun is often not sufficient at eliminating all surface charge, and additional corrections must be performed. Using the known position of the adventitious carbon (C–C) line in the C 1s spectra at 284.8 eV, charge correction was performed. During the measurements, the samples and electron analyzers were electrically grounded to provide a common reference Fermi level. Differential charging is a concern for semiconductor band offset measurements[41–50] and while use of an electron flood gun does not guarantee that differential charging is not present, our experience with oxides on conducting substrates has been that the differential charging is minimized with the use of an electron gun. Calibrations with and without the gun verified that was the case. This procedure has been described in detail previously.[38]

Reflection electron energy loss spectroscopy (REELS) was employed to measure the bandgap of the SiO_2. This technique works well for the wider gap materials. REELS is capable of analyzing electronic and optical properties of ultrathin gate oxide materials since the low-energy-loss region reflects the valence and conduction band structures.[40,41] As electrons are reflected off the surface, energy is lost at energy bands related to excitation of the substrate's electrons. The excitation from the valence band to conduction band is the lowest energy loss possible by an incident

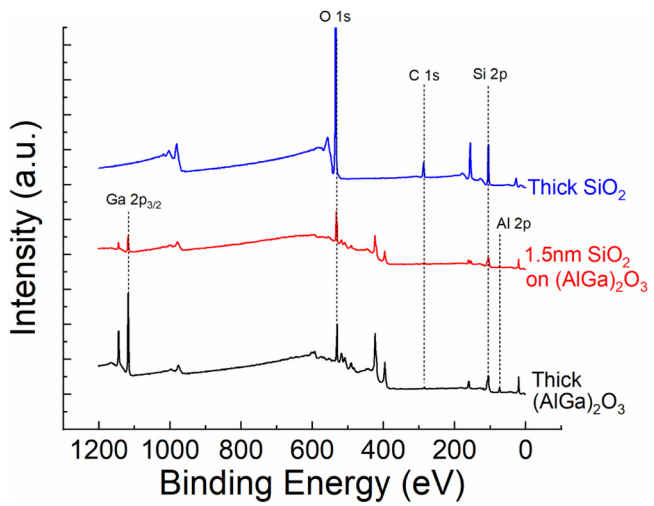

FIG. 2. XPS survey scans of thick ALD SiO_2, 1.5 nm ALD SiO_2 on $(Al_{0.14}Ga_{0.86})_2O_3$, and an $(Al_{0.14}Ga_{0.86})_2O_3$ reference sample. The intensity is in arbitrary units (a.u.).

electron excluding elastic reflection with no energy loss. By taking a linear fit to the leading plasmon peak and finding its zero energy with the background, a direct measurement of valence to conduction band energy is made. REELS spectra were obtained using a 1 kV electron beam and the hemispherical electron analyzer.

III. RESULTS AND DISCUSSION

Figure 2 shows the stacked XPS survey scans of thick (200 nm) SiO_2, 1.5 nm ALD SiO_2 on β-$(Al_{0.14}Ga_{0.86})_2O_3$, and an $(Al_{0.14}Ga_{0.86})_2O_3$ reference sample. The spectra are free from contaminants and consistent with past published XPS data on these materials.[24,34–36] To the detection limit of XPS, there were no metallic contaminants in the films whose oxides might lower the overall bandgap of the dielectrics and thus affect the band alignment. Carbon contamination was minimally present in the thick SiO_2 and 1.5 nm SiO_2 samples which was potentially introduced during the ALD process. The $(AlGa)_2O_3$ reference samples is free from carbon contamination due to being loaded into the XPS system directly after the sample cleaning sequence.

The valence band maximum (VBM) was determined by linearly fitting the leading edge of the valence band and the flat energy distribution from the XPS measurements, and finding the intersection of these two lines,[38,39] as shown in Fig. 3 for (a) the thick SiO_2, and (b) the $(Al_{0.14}Ga_{0.86})_2O_3$. The VBMs were measured to be 3.0 ± 0.2 eV for β-$(Al_{0.14}Ga_{0.86})_2O_3$ and 4.8 ± 0.4 eV for the SiO_2.

The measured band gap for the SiO_2 was 8.7 ± 0.4 eV from the REELS data of Fig. 4(a). As shown in Fig. 4(b), the bandgap of the β-$(Al_{0.14}Ga_{0.86})_2O_3$ was determined to be 5.0 ± 0.3 eV, determined from the onset of the energy loss spectrum.[39] This was used since REELS was not as accurate on the thin layers used here. We should also point out that a similar analysis on the SiO_2 produced a similar bandgap to the REELS result. The difference in bandgaps between SiO_2 and β-Ga_2O_3 is therefore 3.7 eV. The work of Krueger *et al.*[51] determined the compositional dependence of bandgap in $Al_xGa_{1-x}O$ as a linear dependence on Al content, as

$$Eg = (4.75 + 1.87x)\text{eV}.$$

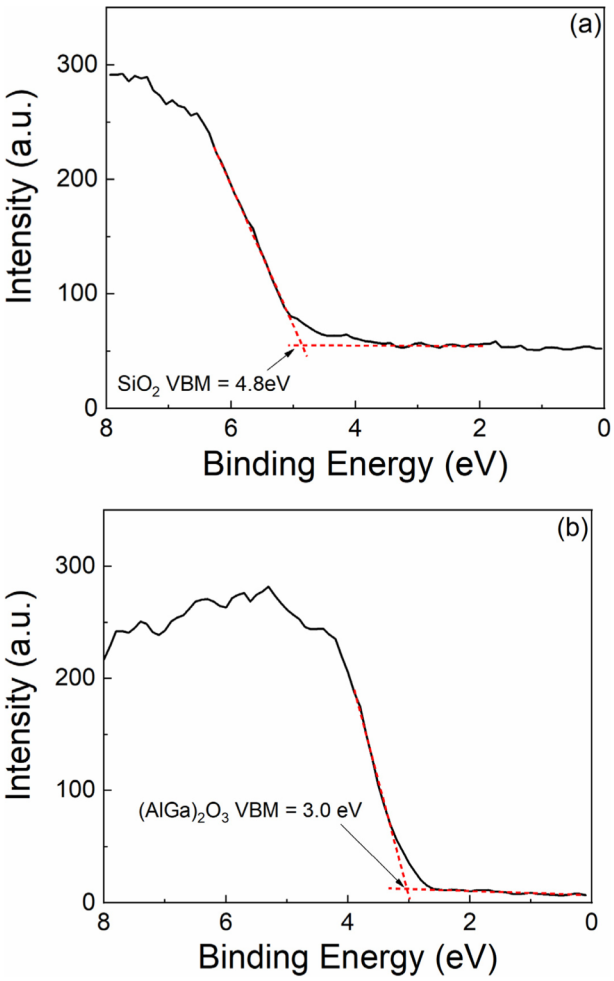

FIG. 3. XPS spectra of core levels to VBM for (a) ALD thick film SiO_2 and (b) reference $(Al_{0.14}Ga_{0.86})_2O_3$.The intensity is in arbitrary units (a.u.).

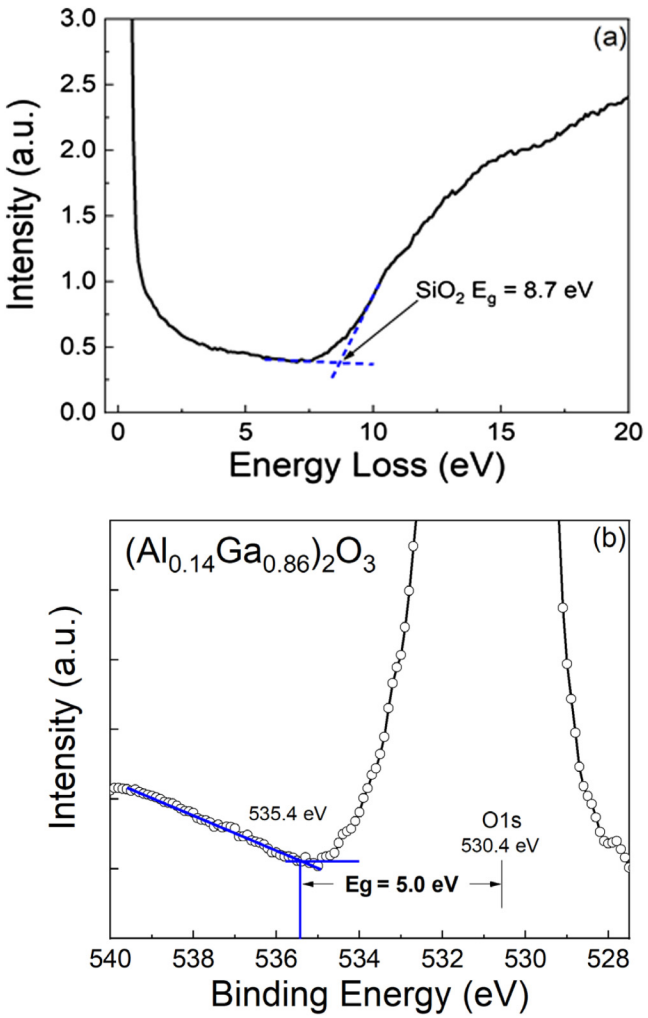

FIG. 4. Bandgap of (a) SiO_2 and (b) $(Al_{0.14}Ga_{0.86})_2O_3$ determined by reflection electron energy loss spectra and the onset of energy loss spectrum, respectively. The intensities are in arbitrary units (a.u.).

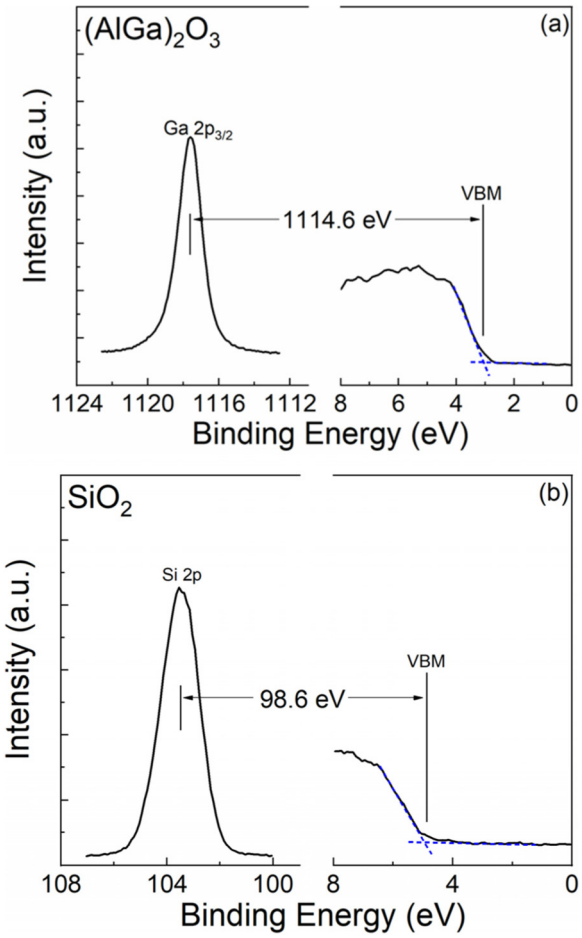

FIG. 5. High resolution XPS spectra for the vacuum-core delta regions of (a) $(Al_{0.14}Ga_{0.86})_2O_3$ and (b) ALD SiO_2. The intensity is in arbitrary units (a.u.).

This would lead to a value of 5.01 eV, consistent with our result. Their data are based on XPS analyses for polycrystalline samples and can be considered as an averaged standard. Wakabayashi *et al.*[23] reported a more pronounced bowing behavior for the compositional dependence of bandgap in $(Al_xGa_{1-x})_2O_3$ alloys, with systematically lower bandgaps at each composition, including pure Ga_2O_3. They suggested this was due to strain in their layers as well as dependence on measurement technique and geometry. Using the equation below, theoretical calculations[24] suggest a dependence of

$$Eg = (1 - x)Eg[Ga_2O_3] + xEg[SiO_2] - bx(1 - x),$$

where b is the bowing parameter with values between 1.78

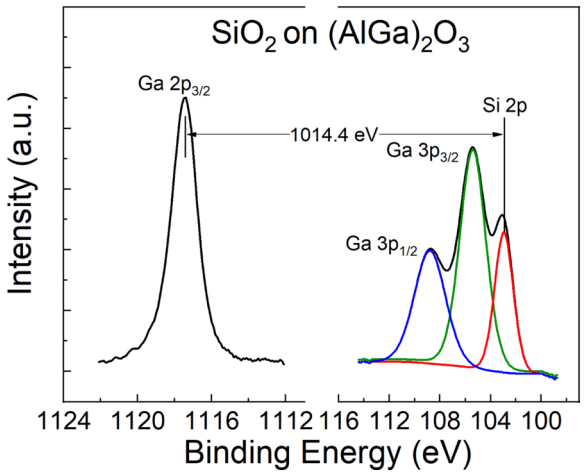

FIG. 6. High resolution XPS spectra for the $(Al_{0.14}Ga_{0.86})_2O_3$ to SiO_2 core delta regions. The intensity is in arbitrary units (a.u.).

and 1.87 eV. For our sample with x = 0.14, this would lead to a bandgap of 5.14 eV.[52]

To determine the band alignment and valence and conduction band offsets, we examined the core level spectra for the samples. Valence band offset is predominantly determined via x-ray photoelectron spectroscopy (XPS) using a method detailed by Kraut *et al.*[39] This method relies on precise measurement of a core level and the valence band edge for each material investigated and measurement in the shift of the core levels when the two materials have formed the heterojunction. Previously, Kraut *et al.*[39] used a valence band density of states fitting for precise measurement of the valence band edge; however, using a linear extrapolation method has been demonstrated to be just as accurate and less intensive. The equation used to calculate the offset is

$$\Delta E_V = (E^1_{core} - E^1_{VBM}) - (E^2_{core} - E^2_{VBM}) - (E^1_{core} - E^2_{core}).$$

Selection of a core level which is well defined and as close as possible in energy to the heterojunction is preferred, because the offsets are small compared to the core level energy and more deviation is expected at higher core level energies.

High resolution XPS spectra of the VBM-core delta region are shown in Fig. 5(a) for the β-$(Al_{0.14}Ga_{0.86})_2O_3$ and thick ALD SiO_2 (b) samples. These were used to determine the selected core level peak positions. Figure 6 shows the XPS spectra for the β-$(Al_{0.14}Ga_{0.86})_2O_3$ to SiO_2 core delta

TABLE I. Summary of measured core levels in these experiments (eV).

Reference $(AlGa)_2O_3$				Reference SiO_2				Thin SiO_2 on $(AlGa)_2O_3$	
Core level	VBM	Core level peak	Core—VBM	Core level	VBM	Core level peak	Core—VBM	Δ core level Ga $2p_{3/2}$—Si 2p	Valence band offset
Ga $2p_{3/2}$	3.00	1117.60	1114.60	Si 2p	4.80	103.40	98.60	1014.40	1.6

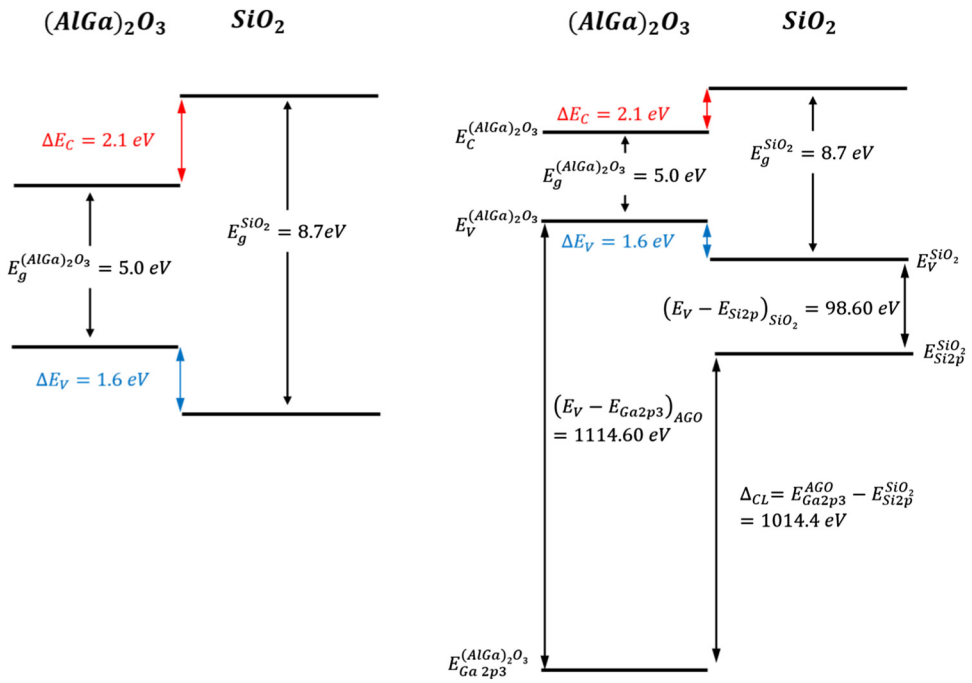

FIG. 7. Summary (left) and detailed (right) band diagrams for the $SiO_2/(Al_{0.14}Ga_{0.86})_2O_3$ heterostructure in which the SiO_2 was deposited by ALD. The valence band offset was determined to be 1.60 ± 0.40 eV for ALD SiO_2 on β-$(Al_{0.14}Ga_{0.86})_2O_3$. The conduction band offset was 2.10 ± 0.08 eV.

regions of the heterostructure samples. These values are summarized in Table I and were then used to calculate ΔE_v.

Figure 7 shows the band alignment of the SiO_2/β-$(Al_{0.14}Ga_{0.86})_2O_3$ heterostructure. This is a nested, type I system with a valence band offset of 1.60 ± 0.40 eV and conduction band offset of 2.10 ± 0.08 eV for the SiO_2/β-Ga_2O_3 system using the relationship

$$\Delta E_C = E_g^{SiO_2} - E_g^{AlGaO} - \Delta E_V, \text{ i.e., } \Delta E_C = 8.7\ \text{eV} - 5.0\ \text{eV} - 1.60\ \text{eV} = 2.10\ \text{eV}.$$

The valence band offset is large enough to provide effective hole confinement, and the conduction band offset is well above the desirable value of 1 eV for good electron confinement, providing a strong resistance to electron transport even at high temperature device operation. Additional dielectrics should be examined, especially as higher Al content β-$(Al_xGa_{1-x})_2O_3$ is developed for heterostructure transistors.

Feng *et al.*[25] reported band alignments of SiO_2/$(Al_xGa_{1-x})_2O_3$ films grown by pulsed laser deposition over the composition range $0 \le x \le 0.49$ and the dielectric deposited by ALD. They also found type I alignments, with similar conduction offsets and smaller valence offsets at our particular Al content. Their conduction band offsets increased from 1.5 to 2.1 eV, respectively, over this composition range while the valence band offsets decreased from 2.2 to 0.9 eV. For some dielectric/semiconductor systems, energy band alignment variations more than 1 eV have reported depending on the interface preparation.[34–38] The interface preparation method influences the band alignment due to the presence of high defect concentrations in the materials and a cation effect that will increase the VBM. These differences are usually seen for the same heterostructure when comparing different deposition methods, i.e., sputtering is more prone to creating interfacial disorder and contributing metallic contamination that affects the bandgap of the dielectric.[38] When comparing the results shown in this study (ALD SiO_2) to Feng's published work (PLD SiO_2), similar offset trends were achieved. Therefore, no significant band alignment differences were noted when comparing SiO_2 films deposited using ALD or PLD. To conclude if growth method impacts the $SiO_2/(Al_xGa_{1-x})_2O_3$ interface, additional studies should be performed using the same Al concentration and substrate growth method. Furthermore, the $SiO_2/(Al_{0.14}Ga_{0.86})_2O_3$ alignment presented in this work is reasonable when compared to previous reports of SiO_2 on undoped Ga_2O_3.

IV. SUMMARY AND CONCLUSIONS

The band alignment at SiO_2/β-$(Al_{0.14}Ga_{0.86})_2O_3$ heterojunctions was obtained from XPS measurements and found to be a nested gap (type I) band offset. The valence band offset was 1.60 eV and the conduction band offset was 2.10 eV. The valence band offset is sufficient for hole confinement, while the conduction band offset provides excellent restriction to electron transport. A comparison of the literature to date on band offsets for dielectrics on β-$(Al_{0.14}Ga_{0.86})_2O_3$ shows no significant variations between material deposited by pulsed laser deposition compared to the MBE-grown samples used here.

ACKNOWLEDGMENTS

The project or effort depicted was partially sponsored by the Department of the Defense, Defense Threat Reduction

Agency, No. HDTRA1-17-1-011, monitored by Jacob Calkins. The content of the information does not necessarily reflect the position or the policy of the federal government, and no official endorsement should be inferred.

[1]A. Kuramata, K. Koshi, S. Watanabe, Y. Yamaoka, T. Masui, and S. Yamakoshi, Jpn. J. Appl. Phys. **55**, 1202A2 (2016).
[2]S. J. Pearton, J. C. Yang, P. H. Cary IV, F. Ren, J. Kim, M. J. Tadjer, and M. A. Mastro, Appl. Phys. Rev. **5**, 011301 (2018).
[3]Masataka Higashiwaki and Gregg H. Jessen, Appl. Phys. Lett. **112**, 060401 (2018).
[4]Z. Galazka *et al.*, ECS J. Solid State Sci. Technol. **6**, Q3007 (2017).
[5]M. Baldini, M. Albrecht, Andreas Fiedler, Klaus Irmscher, Robert Schewski, and Günter Wagner, ECS J. Solid State Sci. Technol. **6**, Q3040 (2017).
[6]Masataka Higashiwaki, Kohei Sasaki, Hisashi Murakami, Yoshinao Kumagai, Akinori Koukitu, Akito Kuramata, Takekazu Masui, and S. Yamakosh, Semicond. Sci. Technol. **31**, 034001 (2016).
[7]S. Oh, J. Kim, Fan Ren, S. J. Pearton, and Jihyun Kim, J. Mater. Chem. C **4**, 9245 (2016).
[8]Kelson D. Chabak *et al.*, Appl. Phys. Lett. **109**, 213501 (2016).
[9]Andrew J. Green *et al.*, IEEE Electron Device Lett. **37**, 902 (2016).
[10]M. J. Tadjer, N. A. Mahadik, V. D. Wheeler, E. R. Glaser, L. Ruppalt, A. D. Koehler, K. D. Hobart, C. R. Eddy, Jr., and F. J. Kub, ECS J. Solid State Sci. Technol. **5**, 468 (2016).
[11]K. D. Chabak *et al.*, IEEE Electron Device Lett. **39**, 67 (2018).
[12]K. Konishi, K. Goto, H. Murakami, Y. Kumagai, A. Kuramata, S. Yamakoshi, and M. Higashiwaki, Appl. Phys. Lett. **110**, 103506 (2017).
[13]W. S. Hwang *et al.*, Appl. Phys. Lett. **104**, 203111 (2014).
[14]Shihyun Ahn, Fan Ren, Janghyuk Kim, Sooyeoun Oh, Jihyun Kim, Michael A. Mastro, and S. J. Pearton, Appl. Phys. Lett. **109**, 062102 (2016).
[15]Janghyuk Kim, Sooyeoun Oh, Michael Mastro, and Jihyun Kim, Phys. Chem. Chem. Phys. **18**, 15760 (2016).
[16]Y. Zhang *et al.*, Appl. Phys. Lett. **112**, 173502 (2018).
[17]S. Krishnamoorthy *et al.*, Appl. Phys. Lett. **111**, 023502 (2017).
[18]E. Ahmadi, O. S. Koksaldi, X. Zheng, T. Mates, Y. Oshima, U. K. Mishra, and J. S. Speck, Appl. Phys. Express **10**, 071101 (2017).
[19]T. Oshima, Y. Kato, N. Kawano, A. Kuramata, S. Yamakoshi, S. Fujita, T. Oishi, and M. Kasu, Appl. Phys. Express **10**, 035701 (2017).
[20]Yuewei Zhang, Chandan Joishi, Zhanbo Xia, Mark Brenner, Saurabh Lodha, and Siddharth Rajan, Appl. Phys. Lett. **112**, 233503 (2018).
[21]Fabi Zhang, Katsuhiko Saito, Tooru Tanaka, Mitsuhiro Nishio, Makoto Arita, and Qixin Guo, Appl. Phys. Lett. **105**, 162107 (2014).
[22]J. C. Yang, Fan Ren, Marko J. Tadjer, and Akito Kuramata, ECS J. Solid State Sci. Technol. **7**, Q92 (2018).
[23]Ryo Wakabayashi, Mai Hattori, Kohei Yoshimatsu, Koji Horiba, Hiroshi Kumigashira, and Akira Ohtomo, Appl. Phys. Lett. **112**, 232103 (2018).
[24]Hartwin Peelaers, Joel B. Varley, James S. Speck, and Chris G. Van de Walle, Appl. Phys. Lett. **112**, 242101 (2018).
[25]Zhaoqing Feng, Qian Feng, Jincheng Zhang, Xiang Li, Fuguo Li, Lu Huang, Hong-Yan Chen, Hong-Liang Lu, and Yue Hao, Appl. Surf. Sci. **434**, 440 (2018).
[26]Y. Jia, K. Zheng, J. S. Wallace, J. A. Gardella, and U. Singisetti, Appl. Phys. Lett. **106**, 102107 (2016).
[27]K. Konishi, T. Kamimura, M. H. Wong, K. Sasaki, A. Kuramata, S. Yamakoshi, and M. Higashiwaki, Phys. Stat. Sol. B **253**, 623 (2016).
[28]T. Kamimura, K. Sasaki, M. H. Wong, D. Krishnamurthy, A. Kuramata, T. Masui, S. Yamakoshi, and M. Higashiwaki, Appl. Phys. Lett. **104**, 192104 (2014).
[29]M. Hattori *et al.*, Jpn. J. Appl. Phys. **55**, 1202B6 (2016).
[30]Virginia D. Wheeler, David I. Shahin, Marko J. Tadjer, and Charles R. Eddy, Jr., ECS J. Solid State Sci. Technol. **6**, Q3052 (2017).
[31]W. Wei, Z. Qin, S. Fan, Z. Li, K. Shi, Q. Zhu, and G. Zhang, Nanoscale Res. Lett. **7**, 562 (2012).
[32]S. H. Chang, Z. Z. Chen, W. Huang, X. C. Liu, B. Y. Chen, Z. Z. Li, and E. W. Shi, Chin. Phys. B **20**, 116101 (2011).
[33]Z. Chen, K. Hishihagi, X. Wang, K. Saito, T. Tanaka, M. Nishio, M. Arita, and Q. Guo, Appl. Phys. Lett. **109**, 102106 (2016).
[34]P. H. Carey, F. Ren, D. C. Hays, B. P. Gila, S. J. Pearton, S. Jang, and A. Kuramata, J. Vac. Sci. Technol. B **35**, 041201 (2017).
[35]P. Carey, F. Ren, D. C. Hays, B. P. Gila, S. J. Pearton, S. Jang, and A. Kuramata, Jpn. J. Appl. Phys. **56**, 071101 (2017).
[36]P. Carey, F. Ren, D. C. Hays, B. P. Gila, S. J. Pearton, S. Jang, and A. Kuramata, Vacuum **142**, 52 (2017).
[37]David C. Hays, B. P. Gila, S. J. Pearton, Andres Trucco, Ryan Thorpe, and F. Ren, J. Vac. Sci. Technol. B **35**, 011206 (2017).
[38]D. C. Hays, B. P. Gila, S. J. Pearton, and F. Ren, Appl. Phys. Rev. **4**, 021301 (2017).
[39]E. A. Kraut, R. W. Grant, J. R. Waldrop, and S. P. Kowalczyk, Phys. Rev. Lett. **44**, 1620 (1980).
[40]E. Bersch, M. Di, S. Consiglio, R. D. Clark, G. J. Leusink, and A. C. Diebold, J. Appl. Phys. **107**, 043702 (2010).
[41]H. C. Shin *et al.*, Surf. Interface Anal. **44**, 623 (2012).
[42]P. H. Carey IV, F. Ren, David C. Hays, B. P. Gila, S. J. Pearton, Soohwan Jang, and Akito Kuramata, Vacuum **141**, 103 (2017).
[43]X. Guo, H. Zheng, S. W. King, V. V. Afanas'ev, M. R. Baklanov, J.-F. D. Marneffe, Y. Nishi, and J. L. Shohet, Appl. Phys. Lett. **107**, 082903 (2015).
[44]A. Zur and T. C. McGill, J. Vac. Sci. Technol. B **2**, 440 (1984).
[45]H.-K. Dong and L.-B. Shi, Chin. Phys. Lett. **33**, 016101 (2016).
[46]J. Xu, Y. Teng, and F. Teng, Sci. Rep. **6**, 32457 (2016).
[47]M. Yang, R. Q. Wu, Q. Chen, W. S. Deng, Y. P. Feng, J. W. Chai, J. S. Pan, and S. J. Wang, Appl. Phys. Lett. **94**, 142903 (2009).
[48]A. Klein, J. Phys: Condens. Matter **27**, 134201 (2015).
[49]A. Klein, Thin Solid Films **520**, 372 (2012).
[50]S. Li *et al.*, Phys. Stat. Sol. Rapid Res. Lett. **8**, 571 (2014).
[51]Benjamin W. Krueger, Christopher S. Dandeneau, Evan M. Nelson, Scott T. Dunham, Fumio S. Ohuchi, and Marjorie A. Olmstead, J. Am. Ceram. Soc. **99**, 2467 (2016).
[52]A. Oulianov, R. A. Crowell, D. J. Gosztola, I. A. Shkrob, O. J. Korovyanko, and R. C. Rey-de-Castro, J. Appl. Phys. **101**, 053102 (2007).